ACS NANO

Cite This: ACS Nano 2018, 12, 4398–4407

www.acsnano.org

ARTICLE

An Optical Technique for Mapping Microviscosity Dynamics in Cellular Organelles

Joseph E. Chambers,[†,∞] Markéta Kubánková,[‡,∞] Roland G. Huber,[§] Ismael López-Duarte,[‡] Edward Avezov,[∥] Peter J. Bond,[§,⊥] Stefan J. Marciniak,[*,†,∞] and Marina K. Kuimova[*,‡,∞]

[†]Cambridge Institute for Medical Research (CIMR), Department of Medicine, University of Cambridge, Wellcome Trust/MRC Building, Hills Road, Cambridge, CB2 0XY, United Kingdom

[‡]Department of Chemistry, Imperial College London, South Kensington, London, SW7 2AZ, United Kingdom

[§]Bioinformatics Institute (BII), Agency for Science, Technology, and Research (A*STAR), Matrix 07-01, 30 Biopolis Street, 138671 Singapore

[∥]UK Dementia Research Institute at the University of Cambridge, Cambridge Biomedical Campus, Cambridge CB2 0AH, United Kingdom

[⊥]Department of Biological Sciences, National University of Singapore, 14 Science Drive 4, 117543 Singapore

Supporting Information

ABSTRACT: **Microscopic viscosity (microviscosity) is a key determinant of diffusion in the cell and defines the rate of biological processes occurring at the nanoscale, including enzyme-driven metabolism and protein folding. Here we establish a rotor-based organelle viscosity imaging (ROVI) methodology that enables real-time quantitative mapping of cell microviscosity. This approach uses environment-sensitive dyes termed molecular rotors, covalently linked to genetically encoded probes to provide compartment-specific microviscosity measurements *via* fluorescence lifetime imaging. ROVI visualized spatial and temporal dynamics of microviscosity with suborganellar resolution, reporting on a microviscosity difference of nearly an order of magnitude between subcellular compartments. In the mitochondrial matrix, ROVI revealed several striking findings: a broad heterogeneity of microviscosity among individual mitochondria, unparalleled resilience to osmotic stress, and real-time changes in microviscosity during mitochondrial depolarization. These findings demonstrate the use of ROVI to explore the biophysical mechanisms underlying cell biological processes.**

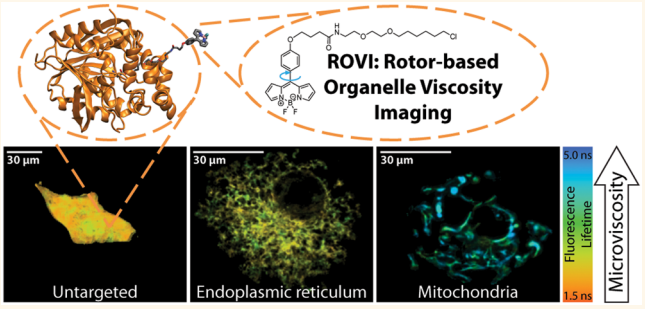

KEYWORDS: *microviscosity, diffusion, organelle, cell biophysics, fluorescence, FLIM, molecular rotors*

The distinct biological functions of cellular organelles are maintained by their endomembrane-mediated compartmentalization, allowing accumulation of macromolecules and small solutes that support specific processes. For example, the endoplasmic reticulum (ER) contains an abundance of molecular chaperones that assist protein folding as well as oligosaccharides and oxidants that promote protein maturation.[1] The abundance and physico-chemical properties of solute molecules affects biophysical properties of organelles, including microviscosity and macromolecular crowding, which are key determinants of diffusion-governed kinetics for countless processes, including protein folding.[2]

Microviscosity governs both the translational and rotational motion of molecules inside a living cell.[2] The biological importance of microviscosity is exemplified in studies showing that changes in plasma membrane microviscosity alter the motility of endothelial cells in response to extracellular growth factors.[3,4] *In vitro* studies have shown the influence of microviscosity on the dynamics of protein folding, protein conformational characteristics,[5] and enzyme kinetics.[6] However, efforts to measure the microviscosity of the specific aqueous intracellular environments where these processes take place have been frustrated by technological limitations. Understanding how microviscosity influences cell biology requires a methodology that provides quantitative and comparable information about distinct cellular environments. Genetically encoded protein probes can be localized to specific subcellular locations. The translational diffusion of fluorescent proteins, measured using techniques such as fluorescence

Received: January 8, 2018
Accepted: April 12, 2018
Published: April 12, 2018

DOI: 10.1021/acsnano.8b00177
ACS Nano 2018, 12, 4398–4407

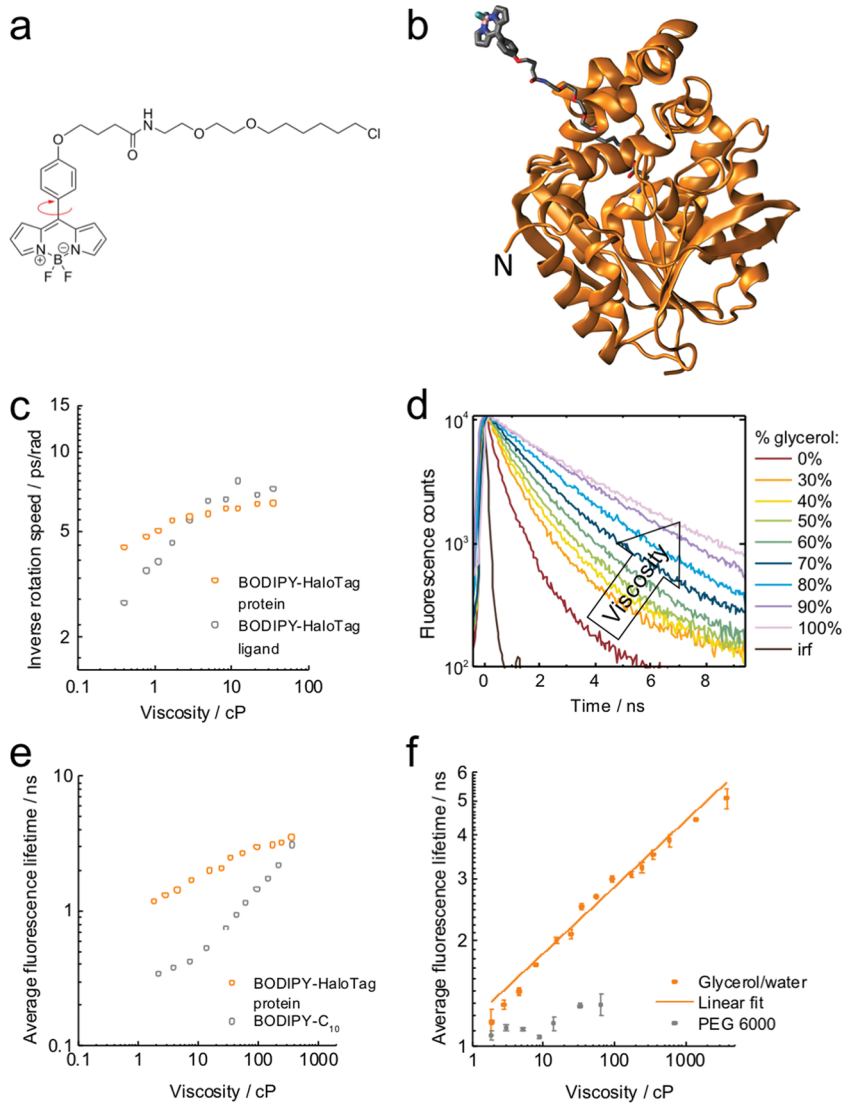

Figure 1. BODIPY-HaloTag structure and viscosity-sensitive photophysics. (a) Chemical structure of BODIPY-HaloTag ligand. (b) Computational model showing the anchoring of a BODIPY-HaloTag ligand to D106 in the channel of HaloTag protein. The protein N-terminus is denoted by "N". (c) *In silico* obtained values of inverse rotational speed of BODIPY moiety as a function of viscosity of water/glycerol mixtures; a comparison of BODIPY-HaloTag protein (orange) and free BODIPY-HaloTag ligand (gray). (d) Fluorescence decays of BODIPY-HaloTag protein in water/glycerol solutions of different concentrations at 37 °C, corresponding to the viscosity range of 1.8−3800 cP. (e) Average fluorescence lifetimes of BODIPY-C_{10} (gray) and BODIPY-HaloTag protein (orange) in various concentrations of water/glycerol solutions with known macroviscosities. (f) Fluorescence lifetime of BODIPY-HaloTag protein in water/glycerol mixtures (orange) and PEG 6000 solutions (gray) at various concentrations (within solubility limits) with known macroviscosity. The relationship between fluorescence lifetime and water/glycerol mixtures viscosity was fit according to the Förster−Hoffmann model (orange line).

recovery after photobleaching (FRAP), has been used to report on the mobility of cellular proteins.[7] However, translational diffusion of a protein is strongly influenced by macromolecular crowding and intracellular compartmentalization, rendering it unsuitable for the assessment of microviscosity. While rotational and translational diffusion of small fluorophores can selectively report microviscosity,[2] a previous inability to localize them to specific compartments precluded their use in measuring microviscosity in such locations.

Small synthetic fluorescent molecules termed "molecular rotors" have emerged as a tool for the measurement of microviscosity in live cells. Molecular rotors respond optically to the microviscosity of the local environment.[8] Both the quantum yield and the fluorescence lifetime of these fluorophores increase with microviscosity-induced hindrance of internal rotation of the molecule.[9] In 2008, Kuimova *et al.*[10] demonstrated experimentally a molecular rotor that reported on intracellular viscosity through its fluorescence lifetime. Fluorescence lifetime is the average time a fluorophore spends in the excited state before emitting a photon and, unlike fluorescence intensity, is a concentration independent parameter. In the case of molecular rotors, a mathematical relationship exists between viscosity and fluorescence lifetime, defined by the Förster−Hoffmann model.[10,11] This framework enables spatial mapping of viscosity using fluorescence lifetime imaging microscopy (FLIM).

While molecular rotors have been directed to cellular locations such as the plasma membranes,[12] mitochondria,[13,14] or endoplasmic reticulum,[15,16] the targeting mechanisms employed have depended upon exploiting the physical and

DOI: 10.1021/acsnano.8b00177
ACS Nano 2018, 12, 4398−4407

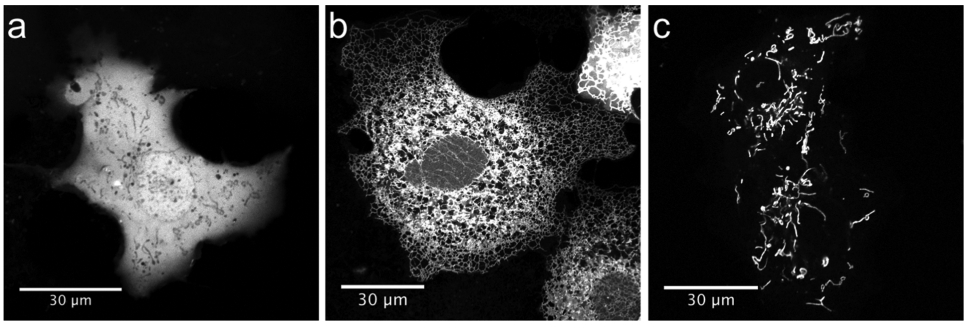

Figure 2. BODIPY-HaloTag probes localize to distinct compartments of cells. COS7 cells were transiently transfected with expression plasmids encoding HaloTag proteins with various organelle localization sequences. HaloTag protein was either (a) untargeted, which accumulated in the cytosol and nucleus, (b) targeted to the ER lumen, or (c) targeted to the mitochondrial matrix. In each case, cells were labeled with 100 nM haloalkane BODIPY ligand for 30 min.

chemical properties of specific endomembranes or by fusion to organelle component proteins. Moreover, the use of chemically distinct probes in different compartments has prevented a true comparison of the reported microviscosities.[12,13,15,17,18] To address this, we sought to develop a multiorganelle targeted microviscosity-sensing system in cells, which we dubbed rotor-based organelle viscosity imaging (ROVI). ROVI combines the microviscosity sensitivity of a molecular rotor with a genetically encoded probe that can be targeted to different cellular compartments with exquisite specificity. Combined with FLIM, this approach provides information on the cellular microviscosity landscape during dynamic biological processes.

RESULTS/DISCUSSION

BODIPY, a molecular rotor based on meso-substituted boron dipyrrin (Figure S1a), emerged as a favorable basis for ROVI design for the following characteristics: a large dynamic range of fluorescence lifetimes (0.4−5.7 ns), corresponding to calibration media macroviscosities of 1−7000 cP (Figure S2), cell permeability,[19] and temperature-independent photophysics.[20]

Cellular proteins localize to distinct subcellular sites by organelle-specific targeting sequences, which are commonly removed enzymatically at their ultimate destination. We sought to apply this targeting system to HaloTag, a protein that covalently binds specific haloalkane-derived synthetic chemical ligands. To test the feasibility of a HaloTag bound microviscosity probe, we used explicitly solvated atomic-resolution molecular dynamics (MD). *In silico* MD simulations provide a physics-based framework to predict, with unparalleled spatiotemporal resolution, the motions of ligands and protein−ligand complexes and their dependence upon local interactions with solvent.[21] Rotational velocities of a haloalkane derivative of BODIPY (Figure 1) were modeled and calibrated to macroviscosity in water/glycerol mixtures (Figure S3a,b). Modeling supported the hypothesis that changes in radiative fluorescence decay are imposed by steric effects on the rate of BODIPY-mesophenyl group rotation[9] (Figure S3c). Simulated viscosity dependence of a haloalkane BODIPY ligand was largely preserved upon covalent attachment to the solved structure of HaloTag protein at D106 (Figure 1b,c). These *in silico* proof-of-principle studies indicated that HaloTag-based organelle targeting could be developed for *in vivo* measurements.

Haloalkane BODIPY ligand (Figure 1a) was synthesized and covalently bound to HaloTag protein *in vitro*, generating a protein-bound viscosity probe as characterized *in silico* (herein referred to as BODIPY-HaloTag) (Figure 1b). The fluorescence lifetime of purified BODIPY-HaloTag responded to small solute-induced changes in microviscosity *in vitro*, with a large dynamic range of 0.75−5.7 ns in water/glycerol mixtures (spanning 37 standard deviations of measurement) corresponding to macroviscosities of 1.8−3800 cP (Figure 1d,e) with negligible temperature sensitivity (Figure S2). BODIPY-HaloTag fluorescence lifetimes were calibrated to water/glycerol standard macroviscosities *via* the Förster−Hoffmann model (see Supporting Information)[11] and described with units of cP relative to glycerol (cP^g) (Figure 1f).

The intracellular milieu is made up of both small solutes and macromolecules, which exert distinct influences on diffusion-limited processes. Small molecule viscogens induce microviscosity effects that perturb diffusion rates. Macromolecules can both perturb diffusion through collision events and generate excluded volume effects that accelerate diffusion limited processes.[22] To test the specificity of ROVI toward these distinct environmental effectors, BODIPY-HaloTag was incubated with solutions of the 6 kDa globular macromolecule polyethylene glycol (PEG) to a concentration of 40% w/w (reflecting the predicted intracellular macromolecular occupancy of 5−40%).[23,24] 6 kDa PEG produced only a modest increase in BODIPY-HaloTag fluorescence lifetime and correlated poorly with macroviscosity of the medium (Figure 1f). A similar trend was seen with 20 kDa PEG, whereas sucrose mixtures produced a strong response in fluorescence lifetime, as seen for glycerol (Figure S4, Figure 1d,e). These data demonstrate BODIPY-HaloTag specificity for small molecule-induced microviscosity, with relative insensitivity to macromolecular crowding.

Next, we assessed the ability of BODIPY-HaloTag to measure intracellular microviscosity. To permit the use of identical fluorophores in distinct organelles, HaloTag coding sequences were modified with N-terminal peptides that target the protein to either the ER or mitochondrial matrix. BODIPY-HaloTag distributions in COS7 cells treated with haloalkane BODIPY ligand were confirmed by confocal microscopy (Figure 2a−c) and colocalized with established organelle markers (Figure S5), while untransfected cells showed negligible fluorescence upon haloalkane BODIPY treatment (Figure S6). BODIPY-HaloTag lacking a targeting sequence accumulated in the cytosol and nucleus where it displayed a mean fluorescence lifetime of 2.37 ± 0.18 ns, corresponding to a microviscosity of ∼39 cP^g (Figure 3a−c and Figure S7A). Of

DOI: 10.1021/acsnano.8b00177
ACS Nano 2018, 12, 4398−4407

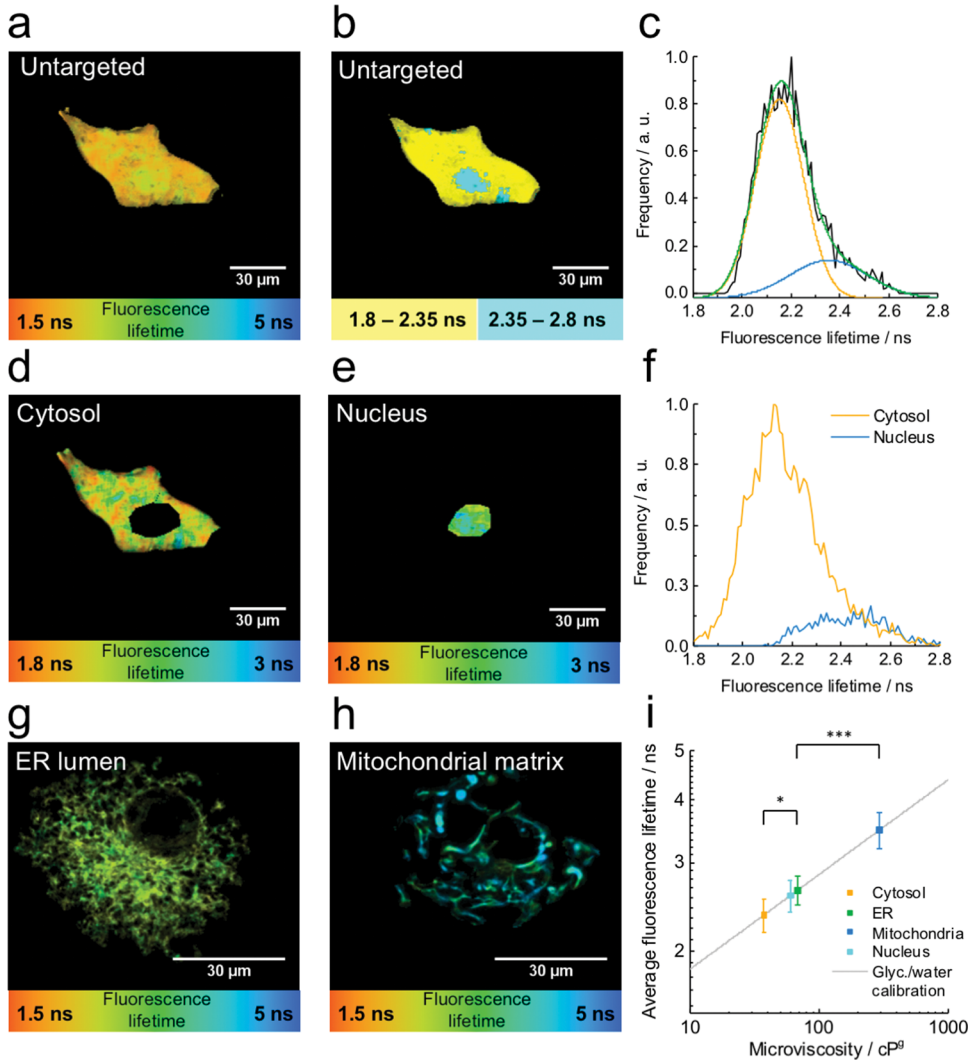

Figure 3. ROVI maps microviscosity in distinct compartments of cells. (a) Color coded fluorescence lifetime image of a COS7 cell expressing BODIPY-HaloTag protein lacking any organelle targeting sequences (Untargeted). Note accumulation throughout the cytosol and nucleus. (b) FLIM image shown in (a) colored with a binary distribution of fluorescence lifetime (Untargeted). (c) Histogram of fluorescence lifetimes of image (a) (black line) fitted with bimodal Gaussian (green), the curves corresponding to the cytosolic lifetime (orange) and nucleosol (blue). (d) Segmented FLIM of cytosol and (e) segmented FLIM of the nucleosol identified by morphology of fluorescence intensity. (f) Histograms corresponding to the segmented FLIMs (d) and (e) in orange and blue, respectively. Note the similar distributions to populations in (c). (g) Lumen of the endoplasmic reticulum. (h) The mitochondrial matrix. (i) Average fluorescence lifetimes of BODIPY-HaloTag protein in the different intracellular localizations at 37 °C overlaying the water/glycerol calibration data with Förster–Hoffmann model fit (gray line). Mean fluorescence lifetimes in the cytosol (11 cells), nucleus (11 cells), ER (10 cells) and mitochondria (18 cells) were analyzed by one-way ANOVA. * $P < 0.05$ (cytosol *vs* ER), *** $P < 0.0001$ (cytosol, nucleus, or ER *vs* mitochondria).

note, this value is higher than previous estimations of cytoplasmic microviscosity of 1–18 cP.[2,25] Bimodal fitting of the fluorescence lifetime distributions of BODIPY-HaloTag lacking a targeting sequence revealed two environments with distinct microviscosities, identified by morphology as the cytosol and nucleus (Figure 3b,c). Individual FLIM analysis of these compartments (Figure 3d-f) revealed a mean cytosolic lifetime of 2.33 ± 0.18 ns and a nuclear mean lifetime of 2.54 ± 0.20 ns, corresponding to microviscosities of ~35 cP^g and ~56 cP^g, respectively (Figure 3i and Figure S7).

Analysis of HaloTag targeted to the ER lumen showed a significantly higher microviscosity than that of the cytosol, with mean lifetime of 2.64 ± 0.17 ns corresponding to ~68 cP^g (Figure 3g,i and Figure S7). Microviscosity within the mitochondrial matrix was dramatically higher than in other compartments, with a mean fluorescence lifetime of 3.54 ± 0.29 ns corresponding to ~325 cP^g (Figure 3h,i). Incubation of purified BODIPY-HaloTag with COS7 cell lysates, dialyzed to remove small molecule cellular viscogens, caused no significant change in probe fluorescence lifetime (Figure S7). This suggests that cellular proteins do not themselves interact with BODIPY-HaloTag in a manner that influences microviscosity measurement. These data showcase the utility of ROVI to resolve biophysically distinct environments in the cell by targeting a single probe to multiple compartments.

Next, we tested the ability of BODIPY-HaloTag to respond to rapid changes in microviscosity induced by osmotic shock. BODIPY-HaloTag expressing COS7 cells grown in isotonic culture medium (305 mOsmol/kg) were briefly exposed to hypotonic conditions (152 mOsmol/kg), leading to visible swelling that was accompanied by a decrease in microviscosity by approximately 34 cP^g (Figure 4a,b,d). Subsequent exposure

DOI: 10.1021/acsnano.8b00177
ACS Nano 2018, 12, 4398–4407

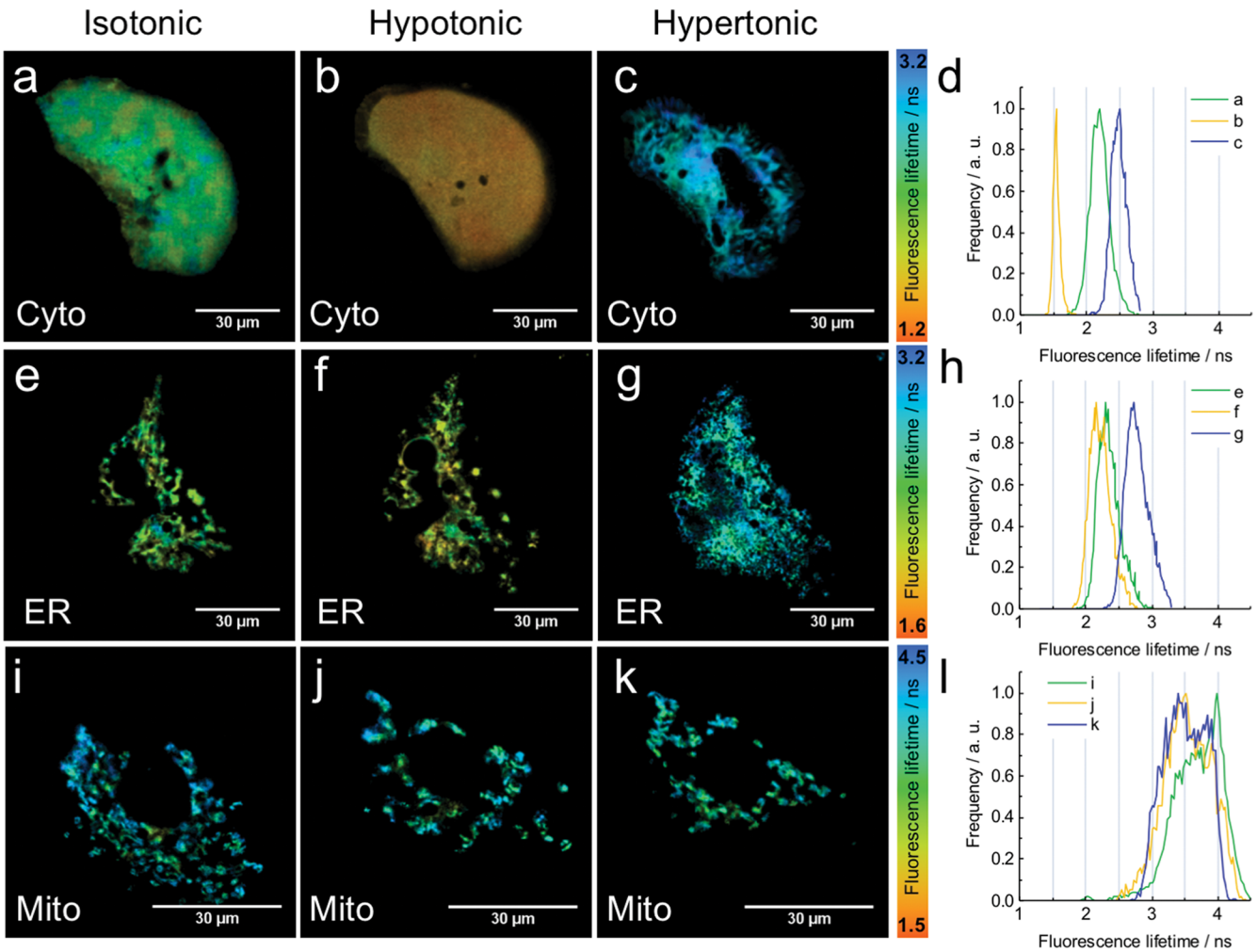

Figure 4. ROVI reveals distinct responses of different subcellular compartments to changes in extracellular osmolality. Color coded FLIM images of BODIPY-HaloTag in COS7 cells expressing HaloTag in (a–c) the cytosol (cyto), (e–g) ER, and (i–k) mitochondrial matrices (mito). Cells imaged in (a,e,i) isotonic, (b,f,j) hypotonic, or (c,g,k) hypertonic culture conditions. Fluorescence lifetime distribution is displayed in histograms for (d) cytosolic, (h) ER, and (l) mitochondrial matrix localized BODIPY-HaloTag. Shown are representative cells from three cells analyzed for each localization.

to hypertonic conditions (609 mOsmol/kg) caused cell shrinkage and a concordant increase in microviscosity 50 cP^g above basal levels (Figure 4c,d). ER microviscosity was modulated by these osmotic changes in line with that of the cytosol (decrease of 41 cP^g in hypotonic and an increase of 35 cP^g in hypertonic conditions), suggesting the two compartments rapidly equilibrate water potential with the extracellular environment (Figure 4e–h). Temporal analysis of ER microviscosity dynamics upon exposure of a cell to hypotonic conditions suggested a single exponential kinetic process (Figure S8a), in line with studies of whole cell swelling under hypotonic conditions.[26] In contrast, mitochondrial matrix microviscosity was relatively stable in the face of hypo- and hyper-osmotic conditions (Figure 4i-l), suggesting that the mitochondrial matrix is insulated from external osmotic shock.

To assess the degree of heterogeneity in microviscosity within cellular compartments, ROVI fluorescence lifetime distribution of individual cells was scrutinized (Figure 5a). Mitochondrial heterogeneity contributed to a significantly broader lifetime distribution than that observed in the cytosol and ER (histogram full-width at half-maximum (fwhm) ~ 1 ns, compared to ~0.3 in the cytosol, ER, or for purified probe at similar fluorescence intensities *in vitro*) (Figure 5a). Mitochondria are structurally dynamic organelles that flux between physically separated compartments and a continuous reticulum by fusion and fission events.[27] Mitochondrial BODIPY-HaloTag imaging revealed a variety of distinct morphologies within individual COS7 cells (Figure 5b and Figure 2c). Matrix viscosities of adjacent mitochondria within a syncytium varied profoundly, exposing matrix discontinuity between physically connected mitochondria that was not revealed by fluorescence intensity (Figure 5b,c).[28] Moreover, mitochondrial lifetime histograms achieved better fit to a bimodal, rather than a single Gaussian distribution (Figure 5c,d), suggesting there are at least two distinct populations of mitochondrial microviscosity in a single cell. Studies in the field of mitochondrial biology have been greatly advanced by the use of pharmacological modulators that have undergone extensive characterization.[29] The relationship between mitochondrial functionality and matrix microviscosity was explored by imaging mitochondria during treatment with one such well-characterized compound, ionomycin, a calcium-specific ionophore that induces collapse of inner mitochondrial membrane polarization and matrix swelling.[30] Treatment of cells with 2 μM ionomycin for 15 min

DOI: 10.1021/acsnano.8b00177
ACS Nano 2018, 12, 4398–4407

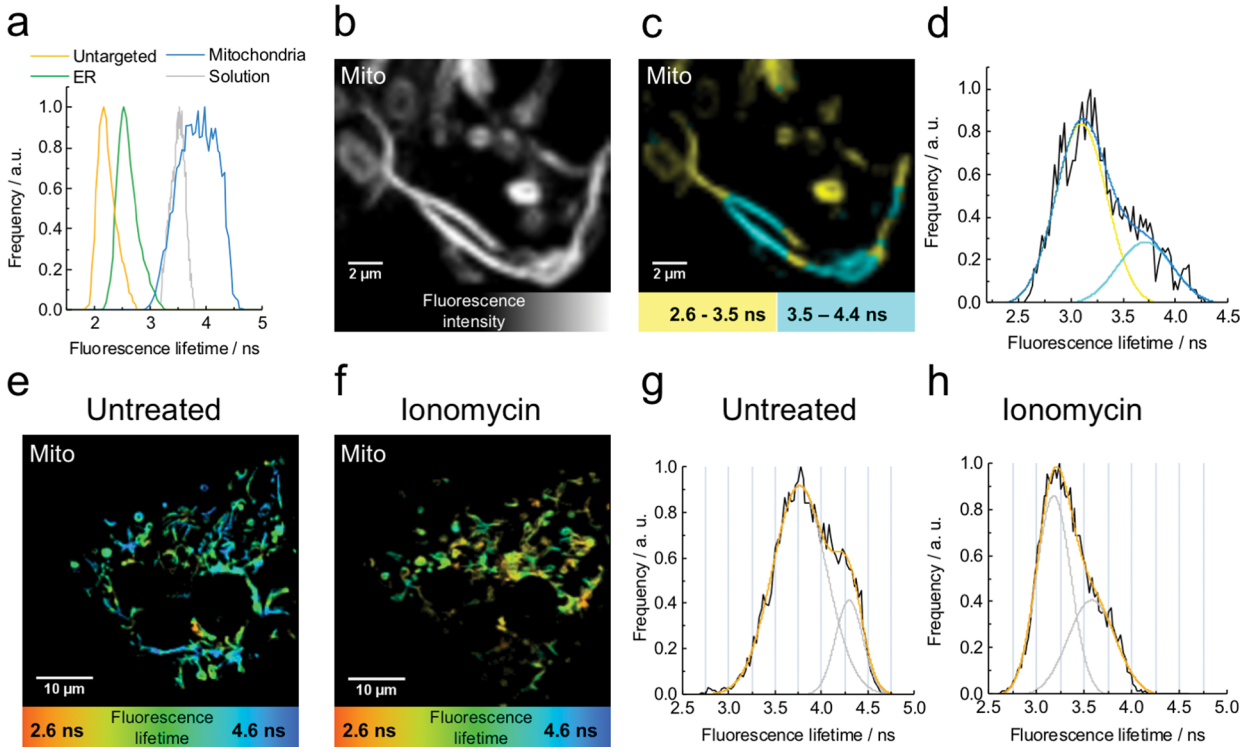

Figure 5. Microviscosity in the mitochondrial matrix is heterogeneous and decreases upon loss of inner membrane potential. (a) Fluorescence lifetime histograms of untargeted, ER-targeted and mitochondrial matrix-targeted BODIPY-HaloTag (corresponding to FLIM images in Figure 3a, g, h, respectively) compared to the fluorescence lifetime histogram of BODIPY-HaloTag in an 80% glycerol calibration mixture at 10 °C (186 cP) recorded at similar FLIM acquisition conditions (Solution). (b) Detail of fluorescence intensity image and (c) FLIM image of BODIPY-HaloTag protein in mitochondrial syncytia (Mito), showing regions of distinct matrix microviscosity. (d) Histogram showing the distribution of fluorescence lifetime in FLIM image (c), including a bimodal Gaussian fit which demonstrates that a minimum of two populations contribute to the fluorescence lifetime. (e) FLIM image of mitochondrial BODIPY-HaloTag in a COS7 cell prior to or (f) after 15 min treatment with 2 μM ionomycin. (g, h) Fluorescence lifetime histograms corresponding to FLIM images (e) and (f), respectively, with bimodal Gaussian fitting. Shown is a representative cell from six cells analyzed.

led to a decrease in lifetime of 0.27 ns ± 0.12 ns, indicating a mean drop in matrix microviscosity of ~130 cP[g] (Figure 5e–h and Figure S7b) upon inner membrane depolarization, that was not seen upon treatment with a DMSO vehicle control. These data provide evidence of changes in matrix microviscosity that accompany alterations in mitochondrial function.

CONCLUSIONS

Endomembrane encapsulation of organelles serves to segregate the molecular contents and environmental properties that endow function to these distinct compartments. The development of biosensors that allow interrogation of organelle properties in live cells has greatly advanced the understanding of a wide range of biological processes. The majority of biosensors report on a specific molecular analyte. The benefits of this type of probe are exemplified by their impact on the understanding of calcium storage and dynamics within the endoplasmic reticulum and mitochondria.[31,32] Likewise, the measurement of redox active species using genetically encoded probes has provided insight into redox biology at the level of organelles.[33−35] Typically, such analyte-specific sensors are designed using a biological template, by modifying biomolecules that possess specific molecular affinities. However, the lack of a unified design principle for the development of sensors that report on environmental biophysical characteristics has presented a challenge. Recently breakthroughs have been made, such as the emergence of a technique that measures macromolecular crowding in cells. This parameter contributes to diffusion rates, which govern the majority of cellular processes.[36] Microviscosity is another biophysical parameter that is predicted to affect cellular diffusion. *In vitro* studies have implicated microviscosity as a modulator of fundamental processes such as enzyme catalysis and protein folding,[5,37] emphasizing the acute need to design live-cell microviscosity biosensors.

We have developed BODIPY-HaloTag as a specific microviscosity-sensing reagent suitable for live cell imaging that allows resolution of spatiotemporal variations in microviscosity on a minute time scale relevant to biological processes. *In vitro* measurements using ROVI showed high specificity to microviscosity and were relatively unaffected by macromolecular crowding (Figure 1f and Figure S4). While macromolecular crowding and microviscosity are known to exert distinct effects on the diffusion of solute molecules, the influence of macromolecules on the effective viscosity felt by small molecules, comparable in size to a molecular rotor, remains an area of active investigation. The use of a genetically encoded probe provided specific subcellular localization to ROVI measurements, enabled by covalent binding of a carefully designed BODIPY-based molecular rotor ligand. Yang *et al.* previously accumulated a molecular rotor within mitochondria using a cationic targeting moiety that is attracted by the negative potential of the inner mitochondrial membrane;[13] however, targeting other organelles would have required the

DOI: 10.1021/acsnano.8b00177
ACS Nano 2018, 12, 4398−4407

generation of different probes endowed with distinct chemical properties to drive targeting. Such an approach risks probe-specific sensitivity to microviscosity that prohibits direct comparisons between multiple locations. By contrast, ROVI permits the targeting of identical fluorophore-protein conjugates to each organelle through the use of cleavable targeting motifs. This efficiently excludes any potential confounding effects from adjoining targeting motifs. Our computational study rigorously predicted the effect of increasing microviscosity on the HaloTag-bound ligand excited-state dynamics. The wide dynamic range of measurement afforded by BODIPY-HaloTag uncovered more than a 9-fold variation in microviscosity between cellular compartments, emphasizing the profound difference between the organellar environments.

Most strikingly, the mitochondrial matrix displayed a distinctly high microviscosity compared with other compartments analyzed (Figure 3i). It is tempting to speculate as to the importance of this feature for mitochondrial function, especially in light of the apparent heterogeneity between the individual mitochondria of a cell (Figure 5a–d) and the drop in matrix microviscosity observed upon mitochondrial depolarization (Figure 5e–h). A large number of studies report functional heterogeneity among mitochondria within a single cell.[38,39] As such, it will be prudent to combine ROVI analysis with additional assays that report on the various functionalities of the mitochondria to explore potential relationships with microviscosity in future studies.

Historically, the study of microviscosity in the context of biology has relied heavily on reductionist biochemical approaches. We believe that ROVI provides an important nanoscale tool for understanding how the compartmentalization and dynamics of biophysical properties in distinct organelles dictate the outcome of a wide range of processes, such as protein folding, enzymology, and metabolism in both physiological and pathological settings.

METHODS/EXPERIMENTAL

Simulations. The structure of the HaloTag protein was retrieved from the protein data bank (4KAF). The protein was modeled using CHARMM36 parameters and solvated in TIP4P water. The BODIPY rotor was modeled using CHARMM CgenFF parameters and covalently attached to the HaloTag residue Asp106 *via* an alkyl-PEG linker. The haloalkane BODIPY ligand in isolation and the BODIPY-HaloTag assembly were set up for two sets of independent MD simulations. Simulations were performed using Gromacs-5.1.4. The systems were minimized and using steepest descent for 10,000 steps, followed by 1 ns of equilibration in the NpT ensemble. Heavy atoms were restrained with a harmonic potential of 1000 kJ nm^{-2} during the course of equilibration. Bonds to hydrogen were constrained using the LINCS procedure. The simulation time step was 1 fs. Temperature was kept constant at 310.15 K using a velocity rescale thermostat. Pressure was maintained at 1 bar using a Berendsen barostat. Electrostatics were described using the particle mesh Ewald procedure with a nonbonded cutoff at 1.2 nm. Following equilibration, position restraints were removed, and production simulations were conducted in triplicate with randomized starting velocities. Simulations were conducted at concentrations of 0%, 30%, 40%, 50%, 60%, 70%, 75%, 80%, 85%, 90%, 95%, and 100% (v/v) of glycerol and water. Viscosities were calibrated using nonequilibrium simulations with a cosine-shaped acceleration field added to the simulation box. The viscosities of modeled solvents are about 50% of experimentally observed values. Temperature dependence and the general trends are well conserved within the models. As the viscosity range relevant to these experiments span multiple orders of magnitude, a deviation of 50% is acceptable. To obtain the velocity of orientation change, the orientation of the BODIPY rotor was determined by calculating the vector connecting the phenyl ring with the annealed three-ring system. Subsequently, all angles between the orientation of two adjacent steps were calculated. The inverse of the 80th percentile of this distribution was correlated well with fluorescence life times.

Synthesis and Characterization of BODIPY-HaloTag Ligand. HaloTag Amine (O2) ligand (Figure S1c) was purchased from Promega Corporation. BODIPY-NHS (Figure S1b) was synthesized as published previously.[40] All solvents (spectroscopic grade) and chemicals were purchased from Sigma-Aldrich.

HaloTag Amine (O2) ligand was dissolved in anhydrous DMSO (0.5 mg in 100 μL). A stock solution of BODIPY-NHS was freshly prepared in anhydrous DMSO solution. Constantly stirring at room temperature, DIPEA was added to the solution containing HaloTag ligand to a final concentration of 39.15 mM. Next, NHS-BODIPY was added from the stock solution to a final concentration of 4.35 mM. The reaction mixture consisted of a 3:1 molar ratio of HaloTag ligand to NHS-BODIPY. The reaction mixture was covered in foil and stirred at room temperature for 16 h to enable conjugation. The reaction was quenched with excess glycine.

Mass spectra were carried out using electrospray ionization (ESI) using Waters LCT Premier (ES-ToF)/Acquity i-Class instrument, confirming the formation of BODIPY-HaloTag ligand conjugates: MS (ES-Positive) for $C_{29}H_{38}N_3O_4ClF_2{}^{11}B$: calculated $[M + H]^+$, 576.2612; found $[M + H]^+$ 576.2615.

Protein Expression and Purification from Bacteria. HaloTag bacterial expression construct was generated by PCR-amplification of N-terminally H6-tagged HaloTag cDNA from HaloTag CMV-neo Vector (Promega, USA) into NdeI-SacI sites of pET30a to produce pET30a-HaloTag. One L cultures of BL21 *Escherichia coli* transformed with pET30a-HaloTag were induced with 1 mM IPTG at an optical density of 0.6 at 600 nm and were grown for a further 6 h before harvesting by centrifugation. Cell pellets were lysed in nitrilotriacetic acid (NTA) lysis buffer (50 mM Tris-HCl, pH 7.5, 500 mM NaCl, 0.2% Triton X-100, 10% glycerol, 20 mM imidazole supplemented with 0.2 mM PMSF and complete EDTA-free protease inhibitor cocktail (Roche, US)) by high-pressure homogenization using an EmulsiFlex-C3 (AVESTIN, Canada). Lysate was cleared by centrifugation at 20,000 *g* for 30 min before incubation with 1 mL Ni-NTA beads (QIAGEN) for 2 h at 4 °C. Beads were washed five times with 20 mL NTA lysis buffer supplemented with 30 mM imidazole. HaloTag was eluted in NTA lysis buffer lacking Triton X-100 and supplemented with 500 mM imidazole and dialyzed into HKM buffer (150 mM KCl, 50 mM Hepes, pH 7.5, and 10 mM $MgCl_2$). 222 μM HaloTag protein was incubated with 414 μM haloalkane BOPIDY ligand for 16 h to generate BODIPY-HaloTag. Free ligand was separated from BODIPY-HaloTag by gel filtration using a Centri Pure P2 Zetadex column (Generon, Berks, UK).

Mammalian Cell Culture and HaloTag Transfection. COS7 cells (Sigma-Aldrich, UK) were cultured in Dulbecco's modified Eagle's medium with 4500 mg/L glucose (Sigma-Aldrich, UK) supplemented with 10% fetal calf serum. The coding sequence of H6-HaloTag was amplified by PCR to incorporate a C-terminal KDEL ER retrieval sequence. This product was inserted into a pFLAG-CMV1 vector downstream of sequence encoding the 15 N-terminal amino acids of mouse preprotrypsin that constitute its cleavable ER targeting signal peptide. Untargeted HaloTag construct was generated by deletion of the ER signal peptide sequence by site-directed mutagenesis PCR. The coding sequence of HaloTag-KDEL was amplified by PCR and inserted in place of the HyPer coding sequence in pHyPer-dMito (Evrogen, Russia) by Gibson assembly, downstream of sequence encoding duplicates of the mitochondrial targeting sequence of human cytochrome c oxidase 8A. Transfections were performed using the Neon Transfection System (Invitrogen, Paisley, UK) applying 1.5 μg of HaloTag mammalian expression vector to 3×10^5 cells, 48 h prior to imaging. An expression vector encoding human protein disulfide isomerase (PDI) fused upstream of mCherry was described previously.[41]

Image Acquisition and Analysis. Confocal images were acquired using a Zeiss 780 confocal microscope. Time-resolved fluorescence decays were collected using time-correlated single-photon counting

DOI: 10.1021/acsnano.8b00177
ACS Nano 2018, 12, 4398–4407

(TCSPC) technique. A mode-locked femtosecond Ti:sapphire laser (Coherent, Chameleon Vision II) tunable over the 680−1080 nm range (140 fs pulse duration, 80 MHz) was used as an excitation source. Fluorescence lifetime imaging microscopy (FLIM) was performed using a confocal laser scanning microscope (Leica, SP5 II) with the Ti:sapphire laser in two-photon excitation mode operated at 880 nm. Short-pass filters of 700 or 715 nm were used. A PMC-100-1 photomultiplier tube (Hamamatsu) and an SPC-830 single-photon counting card (Becker-Hickl) were used for data acquisition. Fluorescence was collected between 500 and 580 nm. The image acquisition time was usually between 180 and 300 s. Samples were placed in chamber slides (LabTekII Chamber Coverglass) mounted in a microscope chamber heated by a circulating thermostat with feedback control of temperature and 0.2 °C precision (Lauda GmbH, E200). The IRF was obtained by measuring SHG signal from urea crystals on a glass cover slide.

Multiexponential fitting was done in SPCI software (Becker-Hickl) using the nonlinear least-squares method and reconvolution algorithm for finding the best fit. Goodness of fit was judged by the χ^2 value and randomness of residuals. Decay models of fluorescence for all conjugated dyes were judged to be biexponential and followed the equation:

$$I(t) = \sum_{i=1}^{n} \alpha_i \exp\left(\frac{-t}{\tau_i}\right)$$

where I is fluorescence intensity, t is time, and α_i is the amplitude, and τ_i is the fluorescence lifetime of the n exponentially decaying components. Mean fluorescence lifetime was calculated according to the equation:

$$\tau_{avg} = \frac{\sum \alpha_i \tau_i^2}{\sum \alpha_i \tau_i}$$

Data were further processed with OriginPro 8.6. Distributions of fluorescence lifetime were fitted using unimodal or bimodal Gaussian curves, from which the mean values were extracted.

Calibrations in Solvents. Water-glycerol mixtures at 10 °C, 20 °C, 30 °C, and 37 °C were used for the calibration of BODIPY-HaloTag protein fluorescence lifetime at viscosities between 1.8 and 3800 cP; published empirically determined formula were used to calculate viscosity values of glycerol,[42] 6 kDa PEG,[43] 20 kDa PEG,[44] and sucrose.[45] Time-resolved fluorescence measurements were used to produce lifetime/viscosity calibrations of these mixtures as described above.

The lifetime/viscosity calibration plot of BODIPY-HaloTag protein in water-glycerol mixtures was fitted using the Förster−Hoffmann model.[11] The empirically derived equation for the relationship between fluorescence lifetime of BODIPY-HaloTag and solvent viscosity was used to determine values of viscosity in the cellular environment. The equation is as follows:

$$\log(\eta) = \frac{\log(\tau) - 3.076}{0.188}$$

PEG standards of molecular mass 6 kDa and 20 kDa (Sigma-Aldrich) were dissolved at concentrations of 10−40% w/w and measured in chamber slides *via* FLIM for evaluating the response of BODIPY-HaloTag to macromolecular crowding. Lysate was prepared by washing approximately 3×10^7 COS7 cells in PBS prior to harvesting in PBS containing 1 mM EDTA to remove cells from culture dishes. Cells were pelleted by centrifugation at 300 *g* for 5 min, before addition of an equal volume of lysis buffer (Buffer L: 140 mM KCl, 10 mM NaCl, 0.5 mM $MgCl_2$, 1.2 mM $CaCl_2$, 20 mM TRIS pH 7.5, 50% w/v glycerol) supplemented with EDTA-free protease inhibitor cocktail (Roche) and 1 mM PMSF. Cell debris was removed by centrifugation at 16,100 *g* for 15 min, and cleared lysate was dialyzed against buffer L using a 5000 Da cutoff membrane to remove cell-derived small solute molecules. Protein content was determined by Bradford assay calibrated with bovine serum albumin.

Live Cell Imaging. For fluorescence imaging cells were plated on an 8-well chamber slides (LabTekII Chamber Coverglass) in 300 μL of culture media at a plating density of 20,000 cells per well and allowed to grow to confluence for 24 h prior to imaging. Immediately before imaging, cells were incubated with 100 nM of haloalkane BODIPY ligand for 1 h, followed by 3 washing cycles with 0.5 mL DMEM. The mitochondrial matrix stain MitoTracker Deep Red FM (Invitrogen, ThermoFisher) was incubated with cells at 50 nM for 20 min prior to 3 washing cycles in DMEM and subsequent image acquisition. Cells cultured in DMEM were exposed to hypotonic shock by addition of an equal volume of salt-free HANKS buffer (140 mM NaCl, 2.5 mM KCl, 0.5 mM $MgCl_2$, 1.2 mM $CaCl_2$, 5 mM glucose, 10 mM HEPES pH 7.5) and incubation for 10 min prior to image acquisition. Hypertonic shock was induced by addition 1.33 volumes of salt-free HANKS supplemented with 500 mM NaCl to cells in hypotonic buffer conditions. Cells were incubated for a further 5 min prior to image acquisition.

Statistics. Where appropriate, data were analyzed using unpaired Student's *t* test, paired *t* test, or analysis of variance (ANOVA) with a Bonferroni *post hoc* correction test using Prism software (Graphpad software, USA).

ASSOCIATED CONTENT

Supporting Information

The Supporting Information is available free of charge on the ACS Publications website at DOI: 10.1021/acsnano.8b00177.

Molecular structures of BODIPY derivatives and the HaloTag ligand, and ESI mass spectrum of BODIPY-HaloTag ligand conjugates. A comparison of the viscosity-lifetime calibrations of BODIPY-HaloTag protein and BODIPY-C_{10} at different temperatures. Calibration of viscosity models *in silico*. Small solute and macromolecule microviscosity measurements with BODIPY-HaloTag. Colocalization of BODIPY-HaloTag with specific organelle markers in COS7 cells. BODIPY-Halo ligand treatment of untransfected COS7 cells showing negligible staining. Mean fluorescence lifetime distribution of ROVI in cellular organelles. Dynamic changes of organellar microviscosity during osmotic stress and upon treatment with a biologically active small molecule (PDF)

AUTHOR INFORMATION

Corresponding Authors

*E-mail: m.kuimova@imperial.ac.uk.
*E-mail: sjm20@cam.ac.uk.

ORCID

Joseph E. Chambers: 0000-0003-4675-0053
Roland G. Huber: 0000-0001-5093-5988
Peter J. Bond: 0000-0003-2900-098X
Stefan J. Marciniak: 0000-0001-8472-7183

Author Contributions

∞J.E.C. and M.K. contributed equally, and S.J.M. and M.K.K. are joint senior authors. M.K. and J.E.C. designed experiments, performed live cell studies, analyzed data, and wrote the manuscript. M.K. performed *in vitro* fluorescence lifetime measurement of purified BODIPY-HaloTag. I.L.D. synthesized BODIPY NHS ester. E.A. assisted with HaloTag localization studies, generated important reagents, and provided critical reading of the manuscript. R.G.H. and P.J.B. carried out atomic-resolution molecular dynamics simulations of BODIPY-C_{10} and BODIPY-HaloTag. M.K.K. and S.J.M. conceived and oversaw the study as a whole and wrote the manuscript.

DOI: 10.1021/acsnano.8b00177
ACS Nano 2018, 12, 4398−4407

Notes

The authors declare no competing financial interest.

ACKNOWLEDGMENTS

J.E.C. was funded by a grant from the Alpha-1 Foundation. M.K. was funded by an Imperial College President's Ph.D. Scholarship and an EPSRC Doctoral Prize Fellowship. R.G.H. and P.J.B. were funded by A*STAR. E.A. is a UK Dementia Research Institute fellow. S.J.M. was funded by the BLF, the MRC, and the Alpha-1 Foundation. M.K.K. and I.L.D. were funded by the EPSRC in the form of Career Acceleration Fellowship to MKK (EP/I003983/1). We thank Alison Schuldt and David Ron for critical reading of the manuscript.

REFERENCES

(1) Braakman, I.; Bulleid, N. J. Protein Folding and Modification in the Mammalian Endoplasmic Reticulum. *Annu. Rev. Biochem.* **2011**, *80*, 71−99.
(2) Kao, H. P.; Abney, J. R.; Verkman, A. S. Determinants of the Translational Mobility of a Small Solute in Cell Cytoplasm. *J. Cell Biol.* **1993**, *120*, 175−184.
(3) Ghosh, P. K.; Vasanji, A.; Murugesan, G.; Eppell, S. J.; Graham, L. M.; Fox, P. L. Membrane Microviscosity Regulates Endothelial Cell Motility. *Nat. Cell Biol.* **2002**, *4*, 894−900.
(4) Vasanji, A.; Ghosh, P. K.; Graham, L. M.; Eppell, S. J.; Fox, P. L. Polarization of Plasma Membrane Microviscosity During Endothelial Cell Migration. *Dev. Cell* **2004**, *6*, 29−41.
(5) Ansari, A.; Jones, C. M.; Henry, E. R.; Hofrichter, J.; Eaton, W. A. The Role of Solvent Viscosity in the Dynamics of Protein Conformational Changes. *Science* **1992**, *256*, 1796−1798.
(6) Dhar, A.; Samiotakis, A.; Ebbinghaus, S.; Nienhaus, L.; Homouz, D.; Gruebele, M.; Cheung, M. S. Structure, Function, and Folding of Phosphoglycerate Kinase are Strongly Perturbed by Macromolecular Crowding. *Proc. Natl. Acad. Sci. U. S. A.* **2010**, *107*, 17586−17591.
(7) Verkman, A. S. Solute and Macromolecule Diffusion in Cellular Aqueous Compartments. *Trends Biochem. Sci.* **2002**, *27*, 27−33.
(8) Haidekker, M. A.; Theodorakis, E. A. Molecular Rotors−Fluorescent Biosensors for Viscosity and Flow. *Org. Biomol. Chem.* **2007**, *5*, 1669−1678.
(9) Kuimova, M. K. Mapping Viscosity in Cells Using Molecular Rotors. *Phys. Chem. Chem. Phys.* **2012**, *14*, 12671−12686.
(10) Kuimova, M. K.; Yahioglu, G.; Levitt, J. L.; Suhling, K. Molecular Rotor Measures Viscosity of Live Cells Via Fluorescence Lifetime Imaging. *J. Am. Chem. Soc.* **2008**, *130* (21), 6672−6673.
(11) Forster, T.; Hoffmann, G. Viscosity Dependence of Fluorescent Quantum Yields of Some Dye Systems. *Z. Phys. Chem.* **1971**, *75*, 63−76.
(12) Lopez-Duarte, I.; Vu, T. T.; Izquierdo, M. A.; Bull, J. A.; Kuimova, M. K. A Molecular Rotor for Measuring Viscosity in Plasma Membranes of Live Cells. *Chem. Commun.* **2014**, *50*, 5282−5284.
(13) Yang, Z.; He, Y.; Lee, J. H.; Park, N.; Suh, M.; Chae, W. S.; Cao, J.; Peng, X.; Jung, H.; Kang, C.; Kim, J. S. A Self-Calibrating Bipartite Viscosity Sensor For Mitochondria. *J. Am. Chem. Soc.* **2013**, *135*, 9181−9185.
(14) Zhao, M.; Zhu, Y. Z.; Su, J.; Geng, Q.; Tian, X. H.; Zhang, J.; Zhou, H. P.; Zhang, S. Y.; Wu, J. Y.; Tian, Y. P. A Water-Soluble Two-Photon Fluorescence Chemosensor for Ratiometric Imaging of Mitochondrial Viscosity in Living Cells. *J. Mater. Chem. B* **2016**, *4*, 5907−5912.
(15) Lee, H.; Yang, Z.; Wi, Y.; Kim, T. W.; Verwilst, P.; Lee, Y. H.; Han, G. I.; Kang, C.; Kim, J. S. BODIPY-Coumarin Conjugate as an Endoplasmic Reticulum Membrane Fluidity Sensor and Its Application to ER Stress Models. *Bioconjugate Chem.* **2015**, *26*, 2474−2480.
(16) Yang, Z.; He, Y.; Lee, J. H.; Chae, W. S.; Ren, W. X.; Lee, J. H.; Kang, C.; Kim, J. S. A Nile Red/BODIPY-Based Bimodal Probe Sensitive to Changes in the Micropolarity and Microviscosity of the Endoplasmic Reticulum. *Chem. Commun.* **2014**, *50*, 11672−11675.
(17) Gatzogiannis, E.; Chen, Z.; Wei, L.; Wombacher, R.; Kao, Y. T.; Yefremov, G.; Cornish, V. W.; Min, W. Mapping Protein-Specific Micro-Environments in Live Cells by Fluorescence Lifetime Imaging of a Hybrid Genetic-Chemical Molecular Rotor Tag. *Chem. Commun.* **2012**, *48*, 8694−8696.
(18) Wang, C.; Song, X.; Chen, L.; Xiao, Y. Specifically and Wash-Free Labeling of SNAP-tag Fused Proteins with a Hybrid Sensor to Monitor Local Micro-Viscosity. *Biosens. Bioelectron.* **2017**, *91*, 313−320.
(19) Kuimova, M. K.; Yahioglu, G.; Levitt, J. A.; Suhling, K. Molecular Rotor Measures Viscosity of Live Cells *via* Fluorescence Lifetime Imaging. *J. Am. Chem. Soc.* **2008**, *130*, 6672−6673.
(20) Vysniauskas, A.; Balaz, M.; Anderson, H. L.; Kuimova, M. K. Dual Mode Quantitative Imaging of Microscopic Viscosity Using a Conjugated Porphyrin Dimer. *Phys. Chem. Chem. Phys.* **2015**, *17*, 7548−7554.
(21) Dror, R. O.; Dirks, R. M.; Grossman, J. P.; Xu, H.; Shaw, D. E. Biomolecular Simulation: A Computational Microscope for Molecular Biology. *Annu. Rev. Biophys.* **2012**, *41*, 429−452.
(22) Rashid, R.; Chee, S. M.; Raghunath, M.; Wohland, T. Macromolecular Crowding Gives Rise to Microviscosity, Anomalous Diffusion and Accelerated Actin Polymerization. *Phys. Biol.* **2015**, *12*, 034001.
(23) Ellis, R. J.; Minton, A. P. Cell Biology: Join the Crowd. *Nature* **2003**, *425*, 27−28.
(24) Zeskind, B. J.; Jordan, C. D.; Timp, W.; Trapani, L.; Waller, G.; Horodincu, V.; Ehrlich, D. J.; Matsudaira, P. Nucleic Acid and Protein Mass Mapping by Live-Cell Deep-Ultraviolet Microscopy. *Nat. Methods* **2007**, *4*, 567−569.
(25) Puchkov, E. O. Intracellular Viscosity: Methods of Measurements and Role in Metabolism. *Biochem. Moscow Suppl. Ser. A* **2013**, *7*, 270−279.
(26) Maric, K.; Wiesner, B.; Lorenz, D.; Klussmann, E.; Betz, T.; Rosenthal, W. Cell Volume Kinetics of Adherent Epithelial Cells Measured by Laser Scanning Reflection Microscopy: Determination of Water Permeability Changes of Renal Principal Cells. *Biophys. J.* **2001**, *80*, 1783−1790.
(27) Friedman, J. R.; Nunnari, J. Mitochondrial Form and Function. *Nature* **2014**, *505*, 335−343.
(28) Collins, T. J.; Berridge, M. J.; Lipp, P.; Bootman, M. D. Mitochondria are Morphologically and Functionally Heterogeneous Within Cells. *EMBO J.* **2002**, *21*, 1616−1627.
(29) Brand, M. D.; Nicholls, D. G. Assessing Mitochondrial Dysfunction in Cells. *Biochem. J.* **2011**, *435*, 297−312.
(30) Bonora, M.; Morganti, C.; Morciano, G.; Giorgi, C.; Wieckowski, M. R.; Pinton, P. Comprehensive Analysis of Mitochondrial Permeability Transition Pore Activity in Living Cells using Fluorescence-Imaging-Based Techniques. *Nat. Protoc.* **2016**, *11*, 1067−1080.
(31) Brini, M.; Cali, T.; Ottolini, D.; Carafoli, E. Neuronal Calcium Signaling: Function and Dysfunction. *Cell. Mol. Life Sci.* **2014**, *71*, 2787−2814.
(32) Contreras, L.; Drago, I.; Zampese, E.; Pozzan, T. Mitochondria: the Calcium Connection. *Biochim. Biophys. Acta, Bioenerg.* **2010**, *1797*, 607−618.
(33) Belousov, V. V.; Fradkov, A. F.; Lukyanov, K. A.; Staroverov, D. B.; Shakhbazov, K. S.; Terskikh, A. V.; Lukyanov, S. Genetically Encoded Fluorescent Indicator for Intracellular Hydrogen Peroxide. *Nat. Methods* **2006**, *3*, 281−286.
(34) Hanson, G. T.; Aggeler, R.; Oglesbee, D.; Cannon, M.; Capaldi, R. A.; Tsien, R. Y.; Remington, S. J. Investigating Mitochondrial Redox Potential with Redox-Sensitive Green Fluorescent Protein Indicators. *J. Biol. Chem.* **2004**, *279*, 13044−13053.
(35) Melo, E. P.; Lopes, C.; Gollwitzer, P.; Lortz, S.; Lenzen, S.; Mehmeti, I.; Kaminski, C. F.; Ron, D.; Avezov, E. TriPer, an Optical Probe Tuned to the Endoplasmic Reticulum Tracks Changes in Luminal H2O2. *BMC Biol.* **2017**, *15*, 24.

DOI: 10.1021/acsnano.8b00177
ACS Nano 2018, 12, 4398−4407

(36) Boersma, A. J.; Zuhorn, I. S.; Poolman, B. A Sensor for Quantification of Macromolecular Crowding in Living Cells. *Nat. Methods* **2015**, *12*, 227−229.
(37) Gavish, B.; Werber, M. M. Viscosity-Dependent Structural Fluctuations in Enzyme Catalysis. *Biochemistry* **1979**, *18*, 1269−1275.
(38) Kruppa, A. J.; Kishi-Itakura, C.; Masters, T. A.; Rorbach, J. E.; Grice, G. L.; Kendrick-Jones, J.; Nathan, J. A.; Minczuk, M.; Buss, F. Myosin VI-Dependent Actin Cages Encapsulate Parkin-Positive Damaged Mitochondria. *Dev. Cell* **2018**, *44*, 484−499.
(39) Kuznetsov, A. V.; Margreiter, R. Heterogeneity of Mitochondria and Mitochondrial Function Within Cells as Another Level of Mitochondrial Complexity. *Int. J. Mol. Sci.* **2009**, *10*, 1911−1929.
(40) Kubankova, M.; Lopez-Duarte, I.; Bull, J. A.; Vadukul, D. M.; Serpell, L. C.; de Saint Victor, M.; Stride, E.; Kuimova, M. K. Probing Supramolecular Protein Assembly Using Covalently Attached Fluorescent MolecularRotors. *Biomaterials* **2017**, *139*, 195−201.
(41) Avezov, E.; Konno, T.; Zyryanova, A.; Chen, W.; Laine, R.; Crespillo-Casado, A.; Melo, E. P.; Ushioda, R.; Nagata, K.; Kaminski, C. F.; Harding, H. P.; Ron, D. Retarded PDI Diffusion and a Reductive Shift in Poise of the Calcium Depleted Endoplasmic Reticulum. *BMC Biol.* **2015**, *13*, 2.
(42) Cheng, N. S. Formula for the Viscosity of a Glycerol-Water Mixture. *Ind. Eng. Chem. Res.* **2008**, *47*, 3285−3288.
(43) Regupathi, I.; Govindarajan, R.; Amaresh, S. P.; Murugesan, T. Densities and Viscosities of Polyethylene Glycol 6000+Triammonium Citrate plus Water Systems. *J. Chem. Eng. Data* **2009**, *54*, 3291−3295.
(44) Mei, L. H.; Lin, D. Q.; Zhu, Z. Q.; Han, Z. X. Densities and Viscosities of Polyethylene-Glycol Plus Salt Plus Water-Systems at 20 Degrees-C. *J. Chem. Eng. Data* **1995**, *40*, 1168−1171.
(45) Swindells, J. F.; Snyder, C. F.; Hardy, R. C.; Golden, P. E. Viscosities of Sucrose Solutions at Various Temperatures: Tables of Recalculated Values.*Supplement to National Bureau of Standards Circular 440*; National Bureau of Standards: Gaithersburg, MD, 1958; pp 483432−483458.

DOI: 10.1021/acsnano.8b00177
ACS Nano 2018, 12, 4398−4407